Decay Process of a Manipulated Large-Scale Horseshoe Vortex in a Turbulent Boundary Layer

H. Makita,* K. Sassa,† M. Abe,‡ and A. Itabashi‡
Toyohashi University of Technology, Toyohashi, Japan

As a model of the coherent structure, an artificial horseshoe vortex was induced by injecting a pair of small pulsative jets into the bottom of a fully developed turbulent boundary layer from a flat plate beneath. After initial growth, the horseshoe vortex had a configuration similar to that of the natural coherent bulge and was broken up by a single manipulator plate installed parallel to the flow direction in the turbulent boundary layer. The ensemble-averaged data, conditionally sampled on the injection of the jets, gave velocity vector fields and shear stress contour maps around the nonmanipulated and manipulated vortices in each stage of their streamwise decay. The manipulated horseshoe vortex was sliced into two blocks that recombined in the downstream region, but with consequent suppression of the induced shear stress in the core of the manipulated horseshoe vortex. The "large-eddy breakup" method was verified as an efficient drag-reduction scheme.

Nomenclature

ℓ_m	= streamwise span of manipulator plate
L_X, L_Y, L_Z	= streamwise, normal, and spanwise scales of coherent vortices, respectively
S	= overall value of induced shear stress
T_d	= time from rising of driving pulse
T_p	= period of injection
u, v, w	= velocity components
U	= local mean velocity
U_∞	= mean velocity of freestream
X, Y, Z	= streamwise, normal, and spanwise coordinates, respectively
Δ	= induced value
δ	= boundary-layer thickness
τ	= duration of driving pulse

Superscripts

$( )'$	= rms value of the fluctuations
$\langle\ \rangle$	= ensemble-averaged value
$(\bar{})$	= time-averaged value

Introduction

THE study of turbulent boundary-layer control raises many challenging problems. The possibility of the large-eddy breakup (LEBU) method was examined by Yajnik and Acharya[1] and, subsequently, by Corke et al.,[2] Hefner et al.,[3] and Bertelrud et al.[4] The principal purpose of these works focused on optimizing the configuration of a manipulator to accomplish more effective drag reduction.[5] These works are of practical importance, but they have not given much information on the fluid-dynamics mechanisms whereby large-scale coherent motions are controlled by the manipulator. Though a number of measurements have been carried out using conditional sampling methods,[6] we still have only unfixed configurations of the nonmanipulated coherent motions because of their random occurrence in time and location in a turbulent boundary layer.

The present experiment was designed to elucidate the fluid-dynamics effects of a single manipulator plate upon the large-scale coherent structure, usually called a "bulge,"[7] in a turbulent boundary layer. An artificially induced horseshoe vortex was employed as a model of the coherent bulge.[8,9] In order to grasp the decay process of the nonmanipulated and manipulated horseshoe vortices, the velocity vector fields and the shear stress distributions were obtained about the artificial horseshoe vortices based on a simplified conditional sampling method. The results showed the rapid decay of the manipulated horseshoe vortex in detail.

Experimental Setup and Procedure

Figure 1 illustrates the present experimental situation. The experiments were conducted in a blowdown wind tunnel 12 m long. A test section of 420 × 420 mm² in cross section and 6 m in length was located behind a nozzle of contraction ratio of 8.16:1. To keep the freestream velocity U_∞ unchanged, the cross-sectional area was slightly enlarged in the streamwise direction at a rate of 5/1000 in effective radius to streamwise distance ratio. All of the measurements were made at $U_\infty = 5.0$ m/s. The local mean velocity U/U_∞ was uniform within ±0.25%, and the turbulence level u'/U_∞ was less than 0.1% in the freestream region.

A flat plate, made of glass of 6 mm in thickness and about 5.7 m in length, was placed parallel to the tunnel axis. It was placed 70 mm from a short rear sidewall of about 1.0 m in length, and the actual area of the test section was about 350 × 420 mm². The flatness of the plate was adjusted to have

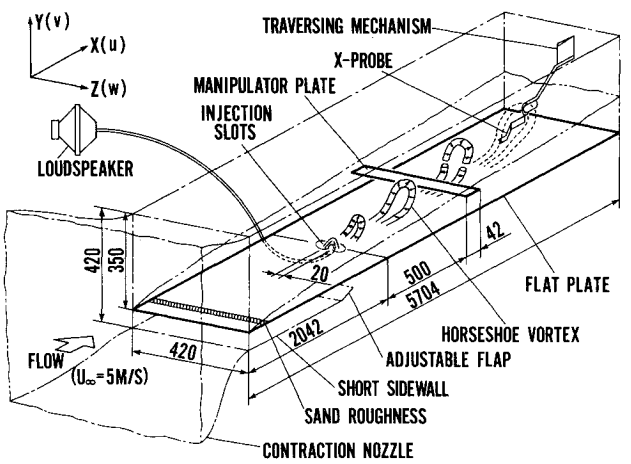

Fig. 1 Schematic diagram of experimental situation (mm).

Presented as Paper 87-1232 at the AIAA 19th Fluid Dynamics, Plasma Dynamics, and Lasers Conference, Honolulu, HI, June 8-10, 1987; received June 18, 1987; revision received May 31, 1988.

*Associate Professor, Department of Energy Engineering.
†Research Student.
‡Graduate Student.

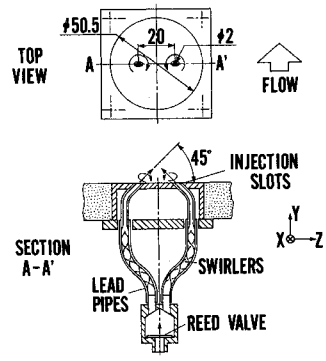

Fig. 2 Details of injection slots (mm).

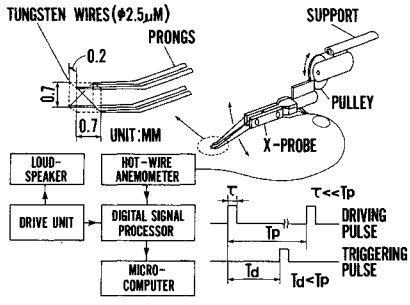

Fig. 3 An adjustable X-wire probe and the block diagram for experiment.

no streamwise pressure gradient through a wall pressure measurement. The plate had a wooden airfoiled leading edge. The inflow condition around the leading edge was determined so as not to cause flow separation by regulating the angle of an adjustable flap at the end of the short rear sidewall. A sand roughness was attached near the leading edge. The boundary layer-thickness δ was about 37.0 mm at injection slots placed 2042 mm downstream of the tip of the leading edge. The Reynolds number based on U_∞ and δ was approximately 1.22×10^4.

A pair of small slots 2.0 mm diam with inward incidence angles of ± 45 deg were placed 20 mm from each other on both sides of the centerline of the flat plate, as shown in Fig. 2. A pair of small jets was intermittently injected from the slots in phase with the pulsation of a loudspeaker driven by the enhancement of an electric pulse. The volume of the jets was about 1.6 cm^3/injection. The jets were given mutually opposite rotation by swirlers in lead pipes. The injected jets were linked with each other at about $Y/\delta = 0.26$ above the centerline ($Z/\delta = 0$) and formed the seed of the vortex with top-spin rotation slightly above the buffer layer. The seed rapidly grew upward to form a large-scale horseshoe vortex at about $X = 500$ mm, where X is the streamwise distance from the injection slots.

As shown in Fig. 1, a thin manipulator plate made of stainless steel of 0.1 mm in thickness was placed parallel to the flat plate at $Y/\delta = 0.7$ and $X = 500$ mm. Its position in height was fitted to the peak location of induced shear stress concentrated in the horseshoe vortex, and it was a little lower than those in preceding works.[3,4] The streamwise span of the plate, $\ell_m = 42$ mm, was chosen to be nearly the same as the boundary-layer thickness[2] at $X = 500$ mm. The manipulator was under tension so that no vibration was observed under the experimental conditions.

The measurements were carried out by constant-temperature hot-wire anemometers and an adjustable X-wire probe made of tungsten wire of 2.5 μm diam. Figure 3 shows the X-wire probe and the block diagram for the experiment. The distance and the right angle between the two wires were adjusted under a microscope. The linearity check of the hot wire and the correction of the attack angle of the probe to the flow direction were made before each measurement.

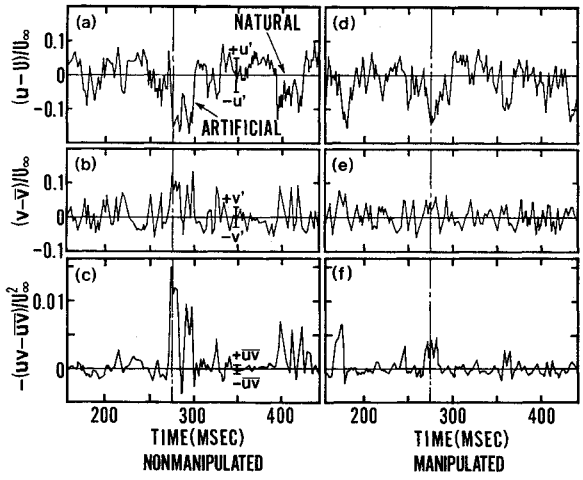

Fig. 4 Instantaneous wave traces of $u - U$, $v - \bar{v}$, and $-(uv - \overline{uv})$ at $X = 1000$ mm, $Y/\delta = 0.7$, and $Z/\delta = 0$; $U_\infty = 5$ m/s; ——·——, $T_d = 275$ ms.

The vortex induction scheme made the conditioning for the data sampling easy. The conditioning was made upon the raising of the triggering pulse properly delayed for T_d from the enhancement of the driving pulse of the loudspeaker, as illustrated in Fig. 3. The interval between the driving pulses, $T_p = 1.3$ s, was set far larger than the pulse duration, $\tau \doteqdot 34$ ms, in order to avoid the interaction between the successively generated horseshoe vortices. Sampled signals were ensemble-averaged 1024 times by a signal processor, and then all of the data were analyzed by a microcomputer.

Results and Discussions

Waveform Observation

The instantaneous waveforms of the streamwise and normal components of the turbulent velocity fluctuation, $u - U$ and $v - \bar{v}$, and the turbulent shear stress $-(uv - \overline{uv})$ detected at $Y/\delta = 0.7$, and $X = 1000$ mm on the symmetry plane ($Z/\delta = 0$) of the artificial horseshoe vortex are shown in Figs. 4a–4c for the nonmanipulated case and in Figs. 4d–4f for the manipulated one. A vertical dashed line in each figure denotes the time mark of $T_d = 275$ ms and is presumed to be the moment when the core of the vortex passes the probe position. A short, vertical solid bar in each figure represents the time-averaged rms amplitude of each turbulent quantity. The rms values were scarcely affected at all by the injection of the swirling jet.

When the horseshoe vortex arrives at the probe position, negative u and positive v are detected. Such a fluid motion is generally called an "ejection" for the natural coherent motion. The intensity and the timewise scale of the artificial ejection are nearly the same as those of the natural one shown on the right-hand side of the same traces. This ensures that the jet injection scarcely damages the structure of the surrounding turbulence field. When the ejection occurs, $-uv$ is enhanced, as shown in Fig. 4c. Its amplitude is larger than that of the natural one, which may be caused by the fact that the induced shear stress concentration in the core of the horseshoe vortex can be exactly detected for the artificial vortex. The ejection is greatly weakened when the vortex is manipulated, and the peak value of the v component decreases to be the same order as that of the background turbulence. Therefore, the direct effect of the manipulation is exerted first on the suppression of the v component.

The ensemble-averaged waveforms of induced quantities $\langle \Delta u \rangle = \langle u \rangle - U$, $\langle \Delta v \rangle = \langle v \rangle - \bar{v}$, and $-\langle \Delta uv \rangle = -(\langle uv \rangle - \overline{uv})$ at $X = 1000$ mm and $Z/\delta = 0$ for various Y positions are shown in Figs. 5a–5c. The solid and broken curves in these figures represent the wave traces for the nonmanipulated and manipulated vortices, respectively. Typical ensemble-averaged

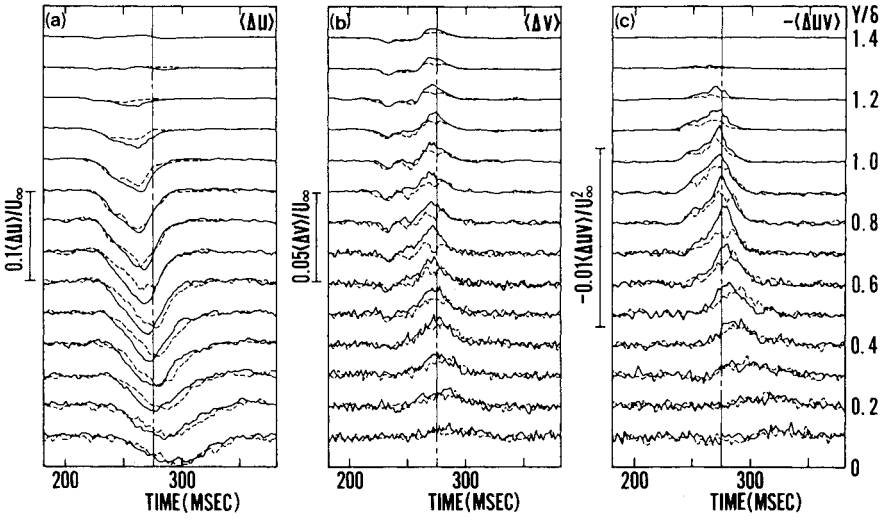

Fig. 5 Ensemble-averaged wave traces of $\langle \Delta u \rangle$, $\langle \Delta v \rangle$, and $-\langle \Delta uv \rangle$ at $X = 1000$ mm and $Z/\delta = 0$; $U_\infty = 5$ m/s; ——, $T_d = 275$ ms; nonmanipulated; ---, manipulated.

Table 1 Scales of artificial and natural vortices

Coherent structure	L_X	L_Y	L_Z	ℓ_m	ℓ_m/L_X
Artificial	5δ	1.3δ	2δ	δ	0.2
Natural	$1 \sim 3\delta$[a]	δ[a]	2δ[b]	$0.5 \sim 1.5\delta$[c]	$0.3 \sim 1.0$[d]

[a]Refs. 7 and 12.
[b]Ref. 11.
[c]Ref. 5.
[d]Estimated from the optimum value $\ell_m = \delta$ in Ref. 5.

patterns are given for these turbulent quantities, although they would be slightly distorted by the vortex jitter,[10] and background scatter is not removed from these traces, especially for $Y/\delta < 0.3$, where the turbulence intensity is high. The patterns of the $\langle \Delta u \rangle$ and $\langle \Delta v \rangle$ traces for the nonmanipulated vortex shown in Figs. 5a and 5b resemble those of the natural coherent bulge given by Fukunishi.[11] The position of the peak or valley in each trace moves more leftward as Y/δ rises, which shows the forward inclination of the artificial horseshoe vortex similar to that of the natural large-scale coherent structure.

Table 1 compares the streamwise, normal, and spanwise scales L_X, L_Y, and L_Z of the natural large-scale coherent structure and the artificial nonmanipulated horseshoe vortex. The values for the artificial vortex were determined from the velocity vector fields presented in the authors' previous work.[9] The present artificial vortex exceeds the natural bulge in L_X, but the other two scales are almost the same between them.[11,12] The difference in L_X may be partly brought about by the fact that only completely formed horseshoe vortices with the largest scales are detected in the present experimental scheme.

The amplitudes of $\langle \Delta u \rangle$, $\langle \Delta v \rangle$, and $-\langle \Delta uv \rangle$ are greatly reduced through the manipulation, as shown in Figs. 5a–5c. The reduction is strong around $Y/\delta = 0.7$, i.e., around the height of the manipulator plate, where the reduction is more effectively made for $\langle \Delta v \rangle$ and $-\langle \Delta uv \rangle$ than for $\langle \Delta u \rangle$. The peak or valley is observed to shift a little rightward in each trace for the manipulated vortex. The amount of the shift increases as Y/δ decreases; that is, the legs of the manipulated vortex are decelerated upstream.

Net Values of the Turbulent Quantities

Figures 6a–6f show the normal distributions of the net values of $\langle u \rangle$, $\langle v \rangle$, and $-\langle uv \rangle$ at several Z/δ of $X = 1000$ mm and $T_d = 275$ ms for the two experimental situations. The time-averaged profiles of U, $\bar{v}$, and $-\overline{uv}$ are also shown by the curves with solid circles in these figures. The profiles of U

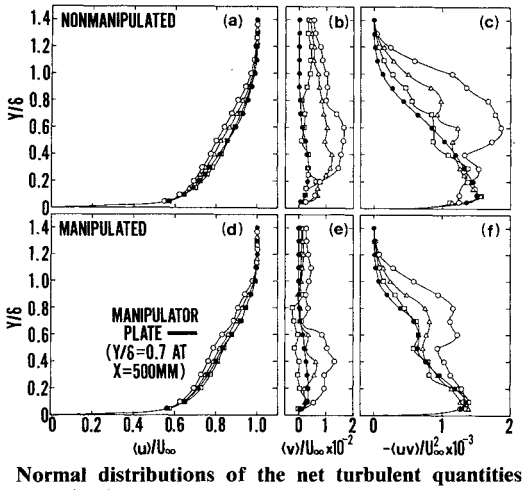

Fig. 6 Normal distributions of the net turbulent quantities $\langle u \rangle$, $\langle v \rangle$, and $-\langle uv \rangle$ at $T_d = 275$ ms detected at $X = 1000$ mm; ●, time-averaged, $Z/\delta = 0$; ○, ensemble-averaged, $Z/\delta = 0$; △, $Z/\delta = 0.2$; □, $Z/\delta = 0.4$; $U_\infty = 5$ m/s.

and $-\overline{uv}$ for the nonmanipulated case coincide closely with those of the ordinary turbulent boundary layer, for example, those measured by Klebanoff.[13] Around $Y/\delta = 0.7$, the net shear stress $-\langle uv \rangle$ is nearly twice as large as the time-averaged value. Accordingly, the ejection can be confirmed to play an important role in the momentum transfer across the turbulent boundary layer.

With the manipulator plate in place, all profiles are obviously distorted. The effect of the manipulation is more remarkable for $\langle \Delta v \rangle$ than for $\langle \Delta u \rangle$, especially in the upper turbulent boundary layer for $Y/\delta > 0.7$. The induced shear stress decreases greatly all across the turbulent boundary layer. The time-averaged shear stress is also suppressed, and the suppression is somewhat restricted, contrary to the case of the ensemble-averaged values, to $Y/\delta < 0.6$. Similar results for the suppression of the time-averaged shear stress were reported by Guezennec and Nagib,[14] who showed that the suppression was related to the "unwinding" of the coherent motion by the vortices generated in the wake of the manipulator plate. Apparently, the unwinding was not observed in the present results. Far more elaborate measurements would be necessary to give the exposition in more detail on the vortex-vortex interaction phenomena near the manipulator plate, and it is a subject for future study.

At $Z/\delta = 0.4$, $\langle \Delta v \rangle$ becomes negative and $\langle \Delta u \rangle$ slightly positive for $Y/\delta < 0.7$, as shown in Figs. 6d and 6e. The distance between the two legs of the horseshoe vortex is known

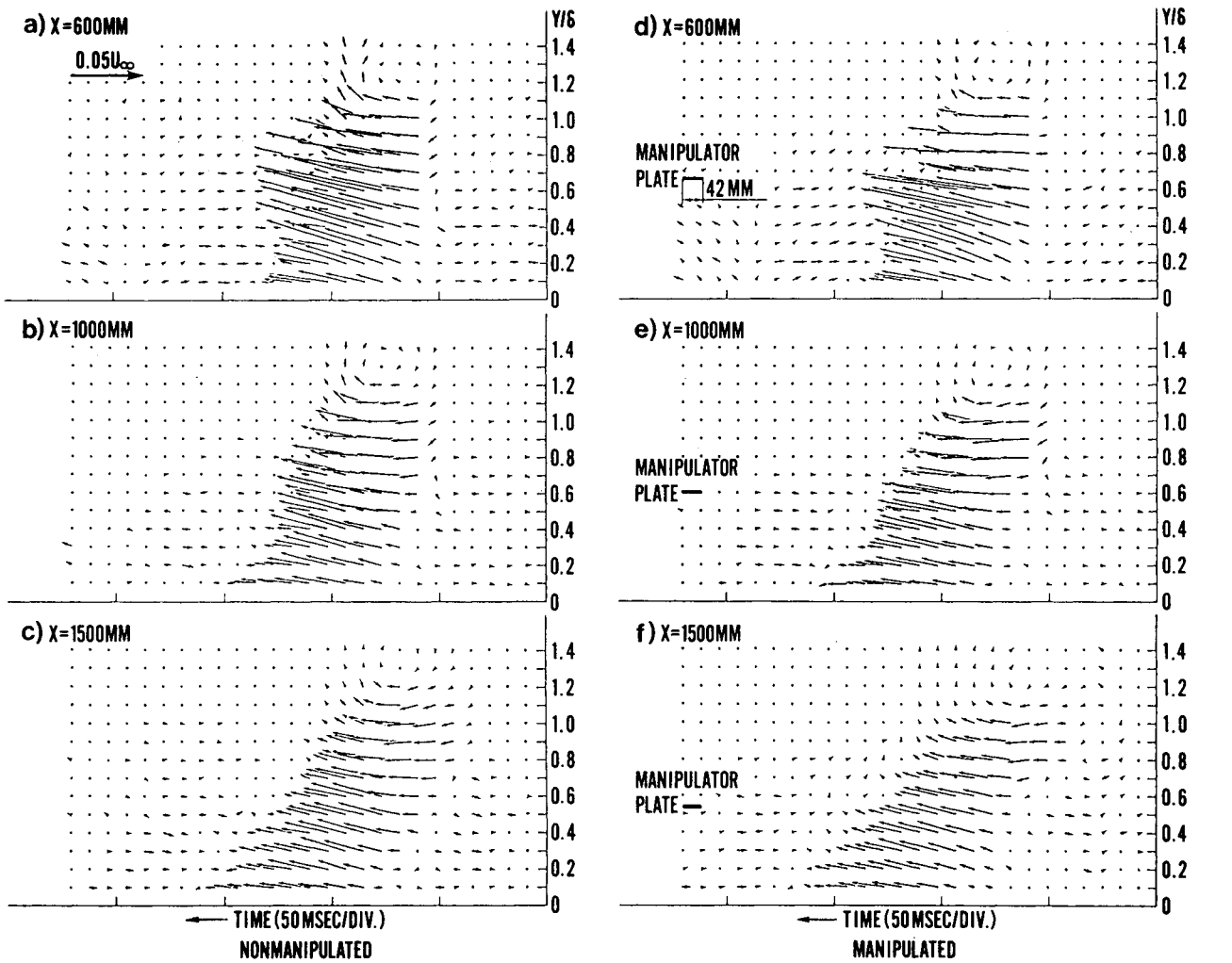

Fig. 7 Induced velocity vector fields about the horseshoe vortex on the symmetry plane ($Z/\delta = 0$); $U_\infty = 5$ m/s.

to be less than 0.8δ under the manipulator plate, in spite of the fact that the distance is a little larger than 0.8δ for the nonmanipulated vortex.

Velocity Vector Fields on Symmetry Plane

In Figs. 7a–7f, velocity vector fields at $Z/\delta = 0$ are illustrated for several streamwise locations of $X = 600$, 1000, and 1500 mm. The arrows in each figure denote the direction and the magnitude of the induced velocity determined from the ensemble-averaged wave traces, as illustrated in Figs. 5. The arrow length equivalent to $0.05U_\infty$ is given on the upper left-hand side of Fig. 7a. The time in these figures passes in the opposite direction to that in Figs. 5, and the right-hand side of each figure is the downstream side. The relative height and span of the manipulator plate are shown by solid short bars on the left-hand sides of Figs. 7d–7f.

The strong ejection covers the region of $Y/\delta < 1.0$ on the symmetry plane ($Z/\delta = 0$) of the nonmanipulated horseshoe vortex at $X = 600$ mm, as demonstrated by Fig. 7a. Contrary to our expectation, a sweep-like motion is not observed anywhere on the symmetry plane. Our result seems to be supported by the recent measurements of Fukunishi[11] but differs from those of other hot-wire measurements[15] and photographic observations.[16,17] These results suggested that the sweep existed all around the coherent structure. Our interpretation is that the sweep occurs chiefly on both sides of the horseshoe vortex and is amplified through the mutual interactions among the neighboring vortices when they are in a close formation, as is usual with natural coherent structures. It appears that the sweep is somewhat more important as the promoter of the turbulent energy in the lower turbulent boundary layer.

The head of the horseshoe vortex (the center of the rotating motion above the strong ejection) exists at about $Y/\delta = 1.3$, which corresponds to the protrusion of the large-scale turbulent bulge to the outside nonturbulent freestream region. As X increases, the head shifts gradually upward, and the horseshoe vortex becomes slightly extended. At the same time, the ejection is gradually weakened.

The vortical motion is evidently controlled by the installation of the manipulator, as shown in Figs. 7d–7f. At $X = 600$ mm, the ejection is strongly suppressed just behind the manipulator plate. The arrows are made shorter, and, as is more typical, their upward angles are greatly reduced around the plate. The ejection is greatly weakened all around the manipulated vortex in the downstream region, as shown by the comparison of Figs. 7b and 7c with 7e and 7f. It should be noted that the manipulated vortex seems to be more inclined forward, and its head moves lower than that of the nonmanipulated one.

The streamwise variation of the height of the head is plotted in Fig. 8, which shows that the nonmanipulated vortex develops rapidly upward before it arrives at the edge of the turbulent boundary layer at about $X = 500$ mm, i.e., in the initial stage of its life. Thereafter, it moves slowly upward at about $Y/\delta = 1.3$ in accordance with the boundary-layer growth. When manipulated, the head moves lower and is not distinguishable for $X > 1500$ mm, although the horseshoe vortex retains a faint sculpture, as described in the following section.

Shear Stress Contours on the Symmetry Plane

In Figs. 9a–9f, the contour maps of the induced shear stress are shown for the two experimental situations. The small islands of negative $-\langle \Delta uv \rangle$ straggling around the horseshoe

vortex are not the regions having really negative shear stress but those with the shear stress relatively lower than the value in the surrounding sections. Figure 9a gives a sculpture of the nonmanipulated horseshoe vortex inclined forward with its head holding slightly up into the nonturbulent freestream region. The peak value of the induced shear stress in the core of the horseshoe vortex decreases as the vortex flows downstream. The nonmanipulated vortex maintains its inherent configuration at $X = 1500$ mm, as shown in Fig. 9c. The locations of the shear stress peak in these figures closely coincide with those where the ejections are most strongly observed in Figs. 7a–7c.

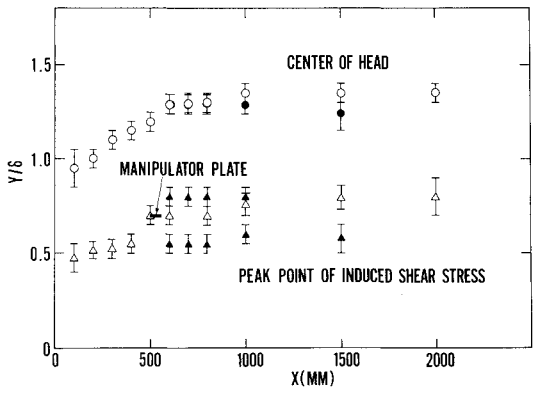

Fig. 8 Streamwise variation of height scales of the horseshoe vortex; center of head: ○, nonmanipulated; ●, manipulated; peak point of induced shear stress: △, nonmanipulated; ▲, manipulated.

As shown in Fig. 9d, the manipulated horseshoe vortex is sliced into two blocks by the manipulator, and these blocks recombined when they arrive at $X = 1000$ mm (see Fig. 9e). In the course of their recombination, the peak intensity in each block is reduced by about 30% of that for the nonmanipulated vortex. The preceding works[14,18] do not mention such recombination. For example, Savill[18] proposed the model as follows: the upper block is rapidly flowed downstream, and the lower block starts to develop again to be a new coherent structure. This difference is caused by the fact that the streamwise scale of the artificial vortex is larger than the span of the manipulator plate for the present experiment. The ratio ℓ_m/L_X is only about 0.2 for the present experiments in spite of $\ell_m/L_X = 0.3 \sim 1.0$ in other works,[5,7,11,12] as shown in Table 1.

Far downstream of the manipulator, the horseshoe vortex has a faint sculpture with slightly greater forward inclination and with its head hanging down. The streamwise change in the height of the peak point of the induced shear stress is shown in Fig. 8. The upper peak position of the manipulated vortex is no more evident at $X = 1500$ mm. As recognized in Fig. 9f, the induced shear stress decreases greatly all around the manipulated horseshoe vortex from that of the nonmanipulated one at $X = 1500$ mm. The manipulated vortex seems already to have lost the ability to preserve its self-consistent configuration, and it has a fragile structure adrift at the mercy of the local mean velocity in the turbulent boundary layer.

Figure 10 illustrates logarithmic plots for the streamwise variation of the overall values of the induced shear stress S on the symmetry plane for both of the present two experimental situations. The overall values are integrated from the local shear stress intensity in the contour maps shown in Fig. 9 as

$$S = \frac{1}{\delta^2} \int\int \frac{-\langle \Delta uv \rangle (X, Y)}{U_\infty^2} \, dX \, dY \tag{1}$$

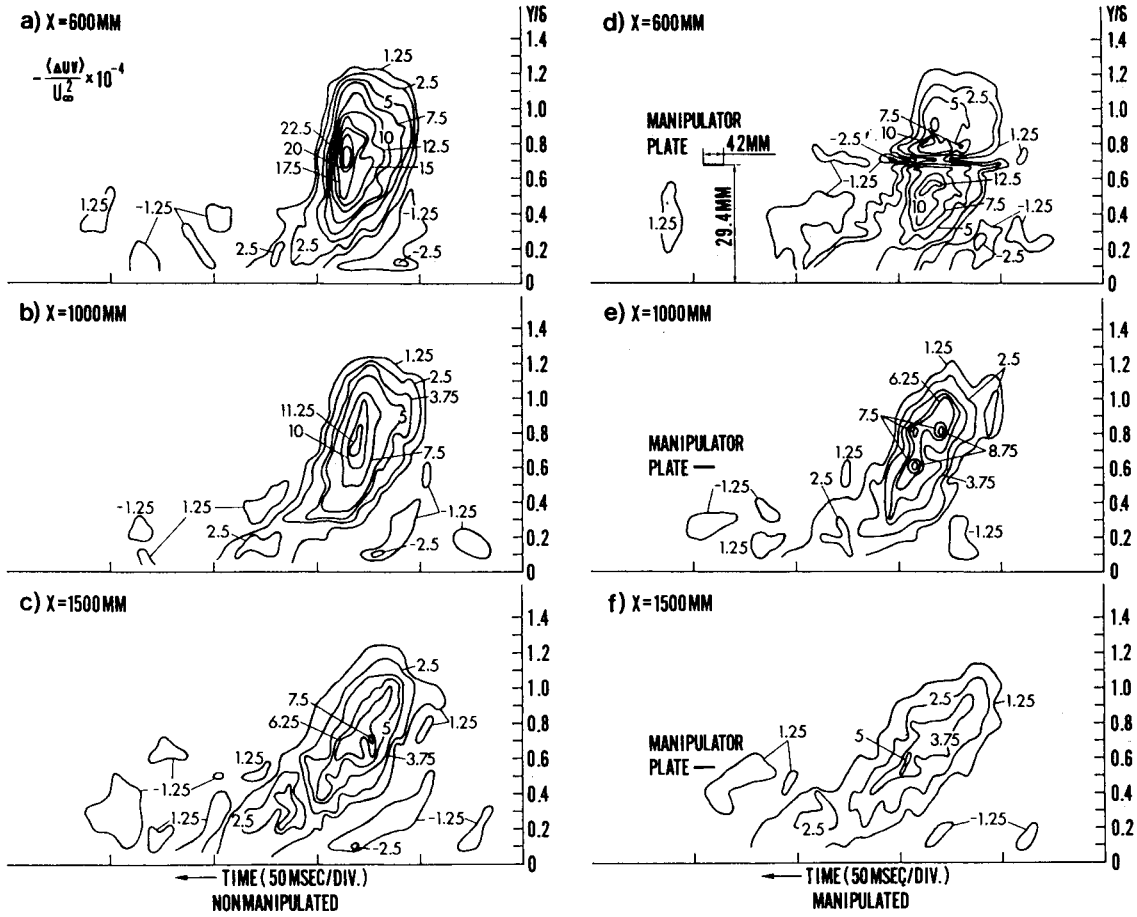

Fig. 9 Contour maps of the induced shear stress about the horseshoe vortex on the symmetry plane ($Z/\delta = 0$); $U_\infty = 5$ m/s.

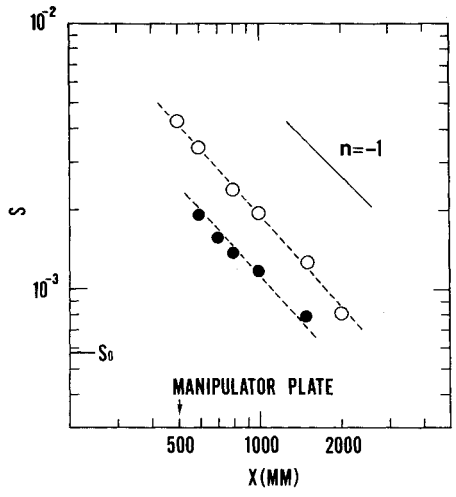

Fig. 10 Streamwise variation of overall value of the induced shear stress on the symmetry plane of the vortex: ○, nonmanipulated; ●, manipulated; S_0, integrated threshold value; $U_\infty = 5$ m/s.

in which dX is given by

$$dX = U(Y) \cdot dT \tag{2}$$

To avoid the ambiguity brought about by the background shear stress scatter, the integration was made with respect to the areas enclosed by the contour lines of $-\langle \Delta uv \rangle / U_\infty^2 \geq 1.25 \times 10^{-4}$: approximately the background level of the induced shear stress. The overall background level $S_0 = 5.78 \times 10^{-4}$, equivalent to the threshold value multiplied by the area at $X = 500$ mm, is marked on the ordinate of the same figure. The overall value for the nonmanipulated horseshoe vortex is known to decrease downstream, and the decay rate n, estimated from the slope of the plots, is almost -1 or a little smaller within the limit of accuracy of the experiment. Insofar as the overall value is concerned, the induced shear stress is suppressed by approximately 40% of the nonmanipulated value just behind the manipulator plate and then decays into the background intensity at almost the same decay rate as the nonmanipulated case in the further downstream region. Such effective reduction in induced shear stress can be related to the efficient restraint of the momentum exchange between the wall surface and the upper freestream region. With these results, the possibility of the drag reduction through the LEBU method is confirmed.

Concluding Remarks

In the present experiment, the effect of the manipulation upon a coherent structure in a fully developed turbulent boundary layer was investigated using an artificially induced horseshoe vortex. The principal results are as follows:

1) The large-scale horseshoe vortex in a turbulent boundary layer is effectively destroyed by a single manipulator plate located at $Y/\delta = 0.7$, where the induced shear stress is most concentrated.

2) The manipulated horseshoe vortex loses its ability to retain its self-consistent configuration and vanishes into the background turbulence rapidly.

3) The ejection on the symmetry plane of the horseshoe vortex is weakened by the manipulation.

4) The overall induced shear stress concentrated in the horseshoe vortex is reduced by approximately 40% of the nonmanipulated value.

5) The net shear stress is also reduced by the manipulation, which assures good utility of the LEBU method as a drag-reduction scheme.

References

[1]Yajnik, K. S. and Acharya, M., "Non-Equilibrium Effects in a Turbulent Boundary Layer Due to the Destruction of Large Eddies," *Structure and Mechanisms of Turbulence I, Lecture Notes in Physics,* Vol. 75, Springer-Verlag, Berlin, 1978, pp. 249–260.

[2]Corke, T. C., Guezennec, Y., and Nagib, H. M., "Modification in Drag of Turbulent Boundary Layers Resulting from Manipulation of Large-Scale Structures," *Progress in Astronautics and Aeronautics: Viscous Flow Drag Reduction,* Vol. 72, edited by G. R. Hough, AIAA, New York, 1980, pp. 128–143.

[3]Hefner, J. N., Weinstein, L. M., and Bushnell, D. M., "Large-Eddy Breakup Scheme for Turbulent Viscous Drag Reduction," *Progress in Astronautics and Aeronautics: Viscous Flow Drag Reduction,* Vol. 72, edited by G. R. Hough, AIAA, New York, 1980, pp. 110–127.

[4]Bertelrud, A., Troung, T. V., and Avellan, F., "Drag Reduction in Turbulent Boundary Layers Using Ribons," AIAA Paper 82-1370, Aug. 1982.

[5]Hefner, J. N., Anders, J. B., and Bushnell, D. M., "Alteration of Outer Flow Structures for Turbulent Drag Reduction," AIAA Paper 83-0293, Jan. 1983.

[6]Antonia, R. A., "Conditional Sampling in Turbulence Measurement," *Annual Review of Fluid Mechanics,* Vol. 13, 1981, pp. 131–156.

[7]Kovasznay, L. S. G., Kibens, V., and Blackwelder, R. F., "Large-Scale Motion in the Intermittent Region of a Turbulent Boundary Layer," *Journal of Fluid Mechanics,* Vol. 41, Pt. 2, 1970, pp. 283–325.

[8]Makita, H. and Sassa, K., "The Structure of Large Scale Vortices Generated by Swirling Jets Ejected into the Turbulent Boundary Layer," *Proceedings of the 16th Turbulence Symposium,* Japan Society of Fluid Mechanics, Tokyo, Japan, 1984, pp. 148–152 (in Japanese).

[9]Makita, H., Sassa, K., and Abe, M., "Structure of a Horse-Shoe Vortex Artificially Induced in a Turbulent Boundary Layer," *Proceedings of the International Conference of Fluid Mechanics,* Peking Univ. Press, Beijing, China, 1987, pp. 104–109.

[10]Zaman, K. B. M. Q. and Hussain, A. K. M. F., "Taylor Hypothesis and Large-Scale Coherent Structures," *Journal of Fluid Mechanics,* Vol. 112, Nov. 1981, pp. 379–396.

[11]Fukunishi, Y., "Influence of Ordered Motions on the Structure of Outer Region of the Turbulent Boundary Layer," *Turbulence and Chaotic Phenomena in Fluids,* North-Holland, Amsterdam, 1984, pp. 371–376.

[12]Cantwell, B. J., "Organized Motion in Turbulent Flow," *Annual Review of Fluid Mechanics,* Vol. 13, 1981, pp. 457–515.

[13]Klebanoff, P. S., "Characteristics of Turbulence in a Boundary Layer with Zero Pressure Gradient," NACA Rept. 1247, 1955.

[14]Guezennec, Y. G. and Nagib, H. M., "Documentation of Mechanisms Leading to Net Drag Reduction in Manipulated Turbulent Boundary Layers," AIAA Paper 85-0519, March 1985.

[15]Brown, G. L. and Thomas, A. S. W., "Large Structure in Turbulent Boundary Layer," *Physics of Fluids,* Vol. 20, Oct. 1977, pp. 243–252.

[16]Falco, R. E., "Coherent Motions in the Outer Region of Turbulent Boundary Layers," *Physics of Fluids,* Vol. 20, Oct. 1977, pp. 124–132.

[17]Offen, G. R. and Kline, S. J., "A Proposed Model of the Bursting Process in Turbulent Boundary Layers," *Journal of Fluid Mechanics,* Vol. 70, Pt. 2, 1975, pp. 209–228.

[18]Savill, A. M., "Effects on Turbulent Boundary Layer Structure of Longitudinal Riblets Alone and in Combination with Outer Layer Devices," *Flow Visualization IV,* Hemisphere, Washington, DC, 1987, pp. 303–308.